Simulations of pressure fluctuations and acoustic emission in hydraulic fracturing

F. Tzschichholz[1,2] and H.J. Herrmann[2,3]

[1] *Division of Physics and Mechanics, School of Technology, Aristotele University of Thessaloniki, 54006 Thessaloniki, Greece*

[2] *HLRZ, Kernforschungsanlage Jülich, Postfach 1913, 5170 Jülich, Germany*

[3] *P.M.M.H. (CNRS, URA 857), École Supérieure de Physique et de Chimie Industrielle de la ville de Paris, 10 rue Vauquelin, 75231 Paris Cedex 05, France*

(Received 27 October 1994)

We consider a two-dimensional lattice model to describe the opening of a crack in hydraulic fracturing. In particular, we consider that the material only breaks under tension and the fluid has no pressure drop inside the crack. For the case in which the material is completely homogeneous (no disorder), we present results for pressure and elastic energy as a function of time and compare our findings with some analytic results from continuum fracture mechanics. Then we investigate fracture processes in strongly heterogeneous cohesive environments. We determine the cumulative probability distribution for breaking events of a given energetical magnitude (acoustic emission). Further, we estimate the probabilty distribution of emission free time intervals. Finally, we determine the fractal dimension(s) of the cracks.

PACS number(s): 05.70.−a, 46.30.−i, 91.60.−x

I. INTRODUCTION

Hydraulic fracturing is widely used in soil mechanics to improve the permeability of reservoirs either in oil recovery or of geothermal wells [1]. Water, an incompressible fluid, is in general, pushed under high pressure deep into the ground by injecting it into a borehole. The fluid penetrates into the solid, opening long cracks. In order to optimize this rather costly procedure, it is crucial to get some deeper understanding of how the fracturing occurs.

In the field it is unfortunately very difficult to obtain direct information about the evolution of the crack in the ground. In present engineering, essentially two types of measurements can be performed: On one hand one can monitor the pressure fluctuations at the injection pump and on the other hand one can register acoustic emission signals on the surface. In two-dimensional Hele-Shaw cells, some controlled laboratory experiments have been performed [2] by injecting water or air into the center of the cell. The resulting cracks display a ramified structure which for high enough pressures is fractal with a dimension of 1.4–1.5.

Using a triangular network of springs and radially stretching the network on the outer boundary into the six directions of a hexagon, the breaking of a material from a central hole was investigated by several authors [3]. They observed fractal cracks having a dimension that depended very much on the type of applied displacements (shear, uniaxial, radial). A stability analysis [4] of the boundary of a circular hole with internal pressure has, however, shown that this case differs considerably from that of a stretched membrane due to the nonlinear dependence of the growth velocity of the crack surface arising from the threshold in cohesion force that must be overcome to break the material.

We have introduced a model [5] in which the imposed load represents a pressure that acts along the entire (inner) surface of the crack in a direction perpendicular to the surface (von Neumann boundary value problem). In this way, the point of application of the imposed load varies during the growth of the crack, a situation that describes the case of hydraulic fracturing more realistically than previous spring models. It also turned out to be more efficient to use a beam model instead of springs. This model had, however, two drawbacks: On one hand the pressure was kept fixed while in real applications it is usually easier to sustain a fixed injection rate. On the other hand, the heterogeneities of the medium were "annealed," i.e., changing in time while the disorder in breaking strength or stiffness in real soils is usually "quenched," i.e., constant on the time scales of the breaking process.

In the present paper we present a model with constant injection rate in which the variations of pressure can be measured and in which the cohesion force is a time independent random variable. We investigate the strong pressure fluctuations and measure the energy release as a function of the statistical distribution of cohesion forces.

II. THE MODEL

In the following we will outline the model employed. First we give a brief description of the basic elastic equations and an explanation of how to incorporate heterogeneous cohesion properties into the fracture model. After this we explain in detail the boundary conditions used. Finally we present the breaking rules we employed which contain the physics of the breaking process considered.

We consider the beam model (as defined on p. 232 of Ref. [6]) on a two-dimensional square lattice of linear size L. Each of the lattice sites i carries three real variables: the two translational displacements x_i and y_i and a rotational angle φ_i. Neighboring sites are rigidly connected

by elastic beams of length l. The beams all have the same cross section and the same elastic behavior, governed by three material dependent constants $a = l/(EA)$, $b = l/(GA)$, and $c = l^3/(EI)$, where E and G are the Young and shear moduli, A the cross section of the beam, and I the moment of inertia for flexion. We used for all simulations the values $a = 1.0$, $b = 0.0017$, and $c = 8.6$. When a site is rotated ($\varphi_i \neq 0$) the beams bend accordingly, always forming tangentially 90° angles with each other. In this way local momenta are taken into account. For a horizontal beam between sites i and j one has the longitudinal force acting at site j, $F_j = \alpha(x_i - x_j)$; the shear force, $S_j = \beta(y_i - y_j) + \frac{\beta}{2} l(\varphi_i + \varphi_j)$; and the flexural torque at site j, $M_j = \frac{\beta}{2} l(y_i - y_j + l\varphi_j) + \delta l^2(\varphi_i - \varphi_j)$, using $\alpha = 1/a$, $\beta = 1/(b + c/12)$, and $\delta = \beta(b/c + 1/3)$. The corresponding equations for vertical beams are similar. In mechanical equilibrium the sum over all internal and external forces (torques) acting on site j must vanish, giving rise in the continuum to the Cosserat equations. We do not consider here inertial or bulk forces such as for gravity.

Before discussing the boundary conditions employed and their physical motivation it is convenient to describe how we included heterogeneous cohesion properties in the fracture model. The concept of local cohesion strength has been used in a number of papers [7]. One assumes that a deformed elastic beam connecting sites i and j always breaks above a certain material specific threshold force f_{coh}^{ij} ("cohesion strength"). If the applied stresses (forces per beam section) are above this threshold the beam breaks and is eliminated, i.e., its elastic moduli are set to zero. Since the cohesional strength for compression is much higher than for tension, we assume [5] that compressed beams can *never* break. If all beams have the same cohesion strength the material is homogeneous. Such homogeneous states are usually investigated in continuum fracture mechanics using the concept of the solid's free surface energy. In the next section we will present some results for equal cohesion thresholds. More realistic, however, is the case in which the breaking thresholds are distributed randomly according to some probability density function, i.e., following a power law, $\rho(f_{coh}) \sim f_{coh}^r$ with $f_{coh} \in [0, f_{max}]$ and $r > -1$. Negative exponents r are used to describe strong cohesive disorder while large positive exponents correspond to weak disorder. It is convenient to express the normalization factor and f_{max} by the distribution's expectation value $\langle f_{coh} \rangle$ and the exponent r. We fixed the average cohesion strength for all simulations to be $\langle f_{coh} \rangle = 0.01$ and investigated the fracture processes for the exponents: $r = -0.7$, $r = -0.5$ (strong disorder) and $r = +\infty$ (no disorder).

Boundary conditions must be defined on the external edges of the lattice and on the internal crack surface. Concerning the external boundary conditions, all displacements and rotations of the sites on the outer edges are assumed to be periodic in horizontal and vertical direction so that the lattice is spanned on a torus. Periodic boundary conditions are preferrable to free boundary conditions because we are interested in asymptotic results for large (infinite) systems. We note that in this case the system cannot expand globally. The second kind of boundary conditions concerns the conditions for forces and torques acting on the inner crack surface. While in tensile experiments the crack surface(s) are always stress free, in hydrodynamic fracturing these surfaces are loaded by a pressure distribution resulting from the invading fluid or gas. In this work we will only consider a homogeneous (spatially constant) pressure distribution acting perpendicular along the entire inner crack surface. However, in contrast to previous simulations [5], here the pressure has strong fluctuations in time. Instead of keeping the inner pressure constant during the simulation we consider the case where the fluid flux ΔV into the crack is constant in time. Hence, the crack opening volume V, which corresponds to the total amount of injected incompressible, fluid increases linearly in time t,

$$V(t) = \Delta V t, \qquad \Delta V = \text{const}\ , \tag{1}$$

a condition which is close to the situation of industrial hydraulic fracturing. For completeness we should mention that the above mentioned equivalence between the crack opening and the injected fluid volume only holds if there is no other sink of fluid in the system besides the crack. Although in practice a loss of fluid in soils is quite common, for the sake of simplicity we do not consider here this effect.

Through Eq. (1) the crack volume V increases in time. We will follow the evolution of the crack growth under the continous increase of loading in the hole. We do this in an iterative way. At each time step the volume increases by a fixed amount ΔV and we estimate from the corresponding elastic solution the stress distribution on the crack surface. According to the breaking rule certain beams can break at a given time step depending on whether or not their stresses are beyond their breaking thresholds. When no beam breaks we continue with the next time step. However, if beams break they are simultanously and irreversibly removed from the set of elastic equations before one proceeds to the next time step. The simulation stops when a certain maximum volume V_{max} is reached. During the simulation we monitor the acting crack pressure, the number of broken beams, and the elastic energy of the system.

In the following we give a more detailed description of the above steps. Our simulation starts at time $t = 1$. At the place into which the incompressible fluid is injected (center of the lattice) one vertical beam connecting sites i and j is removed from the force and momentum balance equations, i.e., the beam is broken. Since we want to simulate the loading of a crack by an injected fluid, a pair of opposite forces (dipole) of unit strength is applied at sites i and j pointing into the elastic bulk. The (unit) pressure is then defined as the acting force per beam length l ($l \equiv 1$). Under the influence of the unit force dipole the lattice becomes distorted. Lattice distortions are in general characterized by the displacement field $\vec{u}(t) = (x_i(t), y_i(t), l\varphi_i(t))$, which, in turn, is determined from the boundary conditions at time t. In the following we will denote by $\vec{u}_0(t)$ the displacement field calculated for a unit pressure P_0. In Ref. [5] we described how to calculate the crack volume V from given

crack surface displacements $\vec{u}$. We denote by $V_0(t)$ the crack volume when computed from $\vec{u}_0(t)$. At time $t = 1$ the injected fluid volume $V(1) = \Delta V$ exerts an equilibrium pressure $P(1) = \Delta V/V_0(1)$ on the crack surface. This follows from the linearity of the elastic equations. The elastic solution which corresponds to this equilibrium pressure is just $\vec{u}(t) = P(t)\vec{u}_0(t)$. We note that this simple relation only holds if the acting pressure can be considered as spatially homogeneous.

We will consider that only beams along the surface of the inner hole can break. In that way only one single crack is generated. At each time step we determine for all beams on the crack surface the force $f^{ij}(t)$ acting along its axis and only if this $f^{ij}(t)$ is positive, i.e., under tension, and larger than the breaking threshold f^{ij}_{coh}, the beam is broken, i.e., its elastic constants α, β, δ are irreversibly set to zero. The forces $f^{ij}(t)$ must be calculated from the actual displacements $\vec{u}(t)$. Note that at a given time step t either several beams can break simultaneously or none break at all. The latter is the case if the stresses of all crack surface beams are below their thresholds. In such a situation the crack volume for unit pressure does not change, $V_0(t+1) = V_0(t)$, because the boundary value problem does not change, i.e., $\vec{u}_0(t+1) = \vec{u}_0(t)$. Hence it is not necessary to recalculate the equilibrium forces. If a certain number of beams breaks simultanously, additional unit force dipoles have to be applied at their corresponding neighboring sites i and j, destroying the previous balance of forces. Then one has to calculate again the internal equilibrium of forces. This is done in our case using a conjugate gradient algorithm with a precision of $\varepsilon = 10^{-10}$ (see Eq. (47) in Ref. [8]). Because of the new boundary conditions the elastic solution changes, i.e., $\vec{u}_0(t+1) \neq \vec{u}_0(t)$, and the volume $V_0(t+1) \neq V_0(t)$ is recalculated from the new crack surface displacements $\vec{u}_0(t+1)$, as described in Ref. [5].

At time $t+1$ the crack pressure takes the value $P(t+1) = V(t+1)/V_0(t+1)$ and the elastic solution matching Eq. (1) is given by $\vec{u}(t+1) = P(t+1)\vec{u}_0(t+1)$. From these displacements one recalculates the forces $f^{ij}(t+1)$ for all beams on the (new) crack surface, decides which are the next beams to be broken, and repeats the procedure described above.

III. FRACTURE OF HOMOGENEOUS SOLIDS

Although homogeneous cohesive properties in solid systems are rather the exception than the rule, it is useful to study them mainly because of their relative simplicity. Our model should be capable of reproducing some general features of simple continuum models for hydraulic fracturing. First we consider the limiting case of equal breaking thresholds $\langle f_{coh} \rangle = f^{ij}_{coh} = 0.01$ for a lattice of linear size $L = 150$. The crack volume (total amount of injected fluid) is increased at a constant rate of $\Delta V = 0.05l^2$ per time step. The simulations stop when the lattices are broken into two pieces. As expected, we find the cracks to have a linear shape. This is due to the fact that the highest stress enhancements occur at the two vertical beams at the tips. Figure 1 shows the time dependence of the pressure P inside the crack in a double logarithmic plot. One can see that on average the pressure drops in time and has oscillations on short time scales. At the beginning, i.e., for time $t = 1$, the crack is very small (one vertical broken beam) and one needs high pressure in order to push the fluid of volume ΔV into the crack. In this particular calculation the two vertical beams on the crack surface are already stressed beyond their cohesion threshold. At the next time step, $t = 2$, these two beams are broken and the pressure drops, because the enlarged crack can now be opened much more easily than before (see Fig. 1). The pressure goes down although additional fluid ΔV has been added to the crack at this time step. It is obvious that a large crack experiences a much lower pressure than a small crack for the same opening volume because the system in that case is locally more stressed. If the pressure drops too much (like at time $t = 2$) the stresses at the two crack tips fall below their cohesion value and the crack cannot grow at the next time step. By injecting more fluid into the crack the pressure increases linearly in time until the cohesion forces can be overcome again. In Fig. 1 one sees a sequence of this oscillating pressure. In the continuum description a smooth decrease of the breaking pressure in time (volume) is expected. Using continuum mechanics one can argue that the smallest pressure necessary to extend the crack at a given opening volume should behave like $P_{crit} \sim V^{-1/3}$ in $d = 2$ [9]. Such a relationship should only hold for an elastic *infinite* plate. Because of Eq. (1) we can identify crack volume with time up to the factor ΔV. For comparison we have plotted in Fig. 1 a dotted line having a slope of $-1/3$. The agreement with our numerical values is quite acceptable over one decade. For short and long times we obtain pronounced deviations which originate from the lattice structure and the finite size of the lattice and from the external boundary conditions.

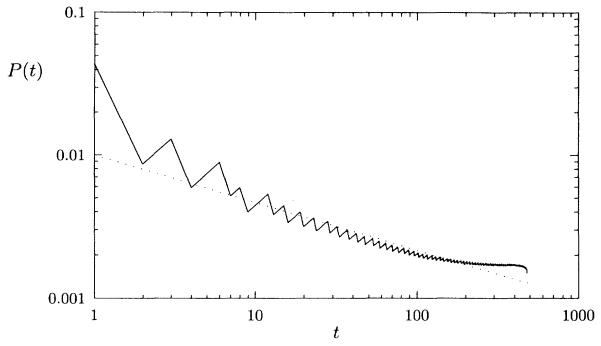

FIG. 1. Log-log plot of the pressure P inside the crack versus time t for homogeneous cohesion ($r \to +\infty$) of strength $\langle f_{coh} \rangle = 0.01$. Points at subsequent time steps are connected by straight lines. The dotted line corresponds to a slope of $-1/3$ as predicted by continuum mechanics. The linear lattice size is $L = 150$.

It is interesting to consider the temporal evolution of the stored elastic energy U. We have calculated the time dependent energy directly by summing up the elastic energies of all nonbroken beams in the system at ev-

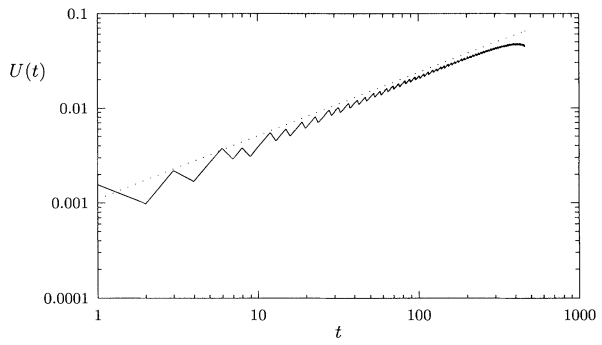

FIG. 2. Log-log plot of the stored lattice energy U versus time t for homogeneous cohesion ($r \to +\infty$) of strength $\langle f_{coh} \rangle = 0.01$. Points at subsequent time steps are connected by straight lines. The dotted line is a guide to the eye of slope 2/3 as predicted by the continuum theory. The lattice size is $L = 150$.

ery time step. In Fig. 2 we show in a log-log plot the time dependence of the elastic energy. Again we see an oscillating behavior as discussed above for the pressure. Breaking events as, for example, at time $t = 1$ and $t = 3$ *decrease* the elastic energy while the elastic energy is *increased* by pushing fluid into the crack. Globally, the elastic energy must increase because the system becomes more compressed in time. We find that the peak energies scale in time as a power law over two and a half decades with an exponent close to 2/3; see Fig. 2. This exponent can be understood by calculating the work $W_{crit} = \int_0^V P_{crit}(V')\ dV'$ done by the external forces in order to inject the fluid volume V, which yields $2U_{crit} = W_{crit} \propto V^{2/3}$. This agrees well with our numerical findings. Again finite size effects lead to deviations from the behavior of an infinite continuum.

IV. CRACKS IN HETEROGENEOUS SOLIDS

In the following we will consider the influence of strongly heterogeneous cohesive strengths on the hydraulic fracturing process. It is well known that fracture processes in disordered solid systems show a rich phenomenology concerning the crack geometry such as, for example, crack branching and crack deflection [6]. There exist phenomena, such as the appearence of microcracks in solids, which cannot be explained by equilibrium thermodynamics without considering the heterogenity of physical properties. Experimental and theoretical investigations during the last decades have established that the overwhelming number of fracture phenomena in solid systems is strongly influenced or even controlled by inhomogeneities.

We will investigate the statistical properties of breaking sequences during hydraulic fracturing and their correlations in space, time, and magnitude. Similar quantities are frequently considered in the analysis of earthquake occurrences [10,11] and of acoustic emission (AE) during microfracturing of rocks [12] or of technical materials [13]. Acoustic emission records for the hydraulic fracturing in geothermal wells have been published for example in Ref. [14].

In our simulations we have considered threshold distributions for two different exponents $r = -0.7$ and $r = -0.5$ (see the preceding section for the definition of the distribution). Figure 3 shows a typical hydraulic crack pattern grown in a medium with strong disorder ($r = -0.7$) on a lattice of linear size $L = 150$. The crack consists of 629 broken beams after 1500 time steps. Apparently, smaller crack branches appear along larger branches, a geometrical property which is typically observed for self-similar (fractal) structures. We have evaluated the fractal dimension(s) of the hydraulic cracks generated by considering the relationship between the typical crack radius $R(N)$ and the number of broken beams N. For this we calculate the squared radius of gyration $R^2(N) = \frac{1}{N}\sum_i (\vec{r}_i - \vec{r}_0)^2$ with $\vec{r}_0 = \frac{1}{N}\sum_i \vec{r}_i$. Finally, the radius $R(N)$ is averaged over a number of independent configurations in order to obtain results for *typical* cracks. In Fig. 4 we show in a log-log plot the number of broken beams N versus the typical crack radius $R(N)$ for the two statistics of the heterogenities characterized by exponents $r = -0.7$ and $r = -0.5$. We find in both cases power laws $N \propto R^{d_f}$ with $d_f > 1$, giving evidence of fractal crack growth. The exponent d_f is called the fractal dimension of the crack and takes for $r = -0.7$ ($\diamond$) and $r = -0.5$ (+) the values $d_f = 1.44 \pm 0.10$, and $d_f = 1.39 \pm 0.10$, respectively. These values for d_f are consistent with the fractal dimension found in the two-dimensional experiments on hydraulic fracturing of viscoelastic clays [2]. One detects, however, from both curves in Fig. 4 a crossover at large R to a lower slope $d_f \approx 1.25$. It is interesting to note that the crossover radii $R_\times$ depend on the width of the threshold distribution. The cracks for stronger disorder $r = -0.7$ show a higher crossover radius $R_\times \approx 18$ than those for $r = -0.5$ with $R_\times \approx 10$. This is qualitatively in agreement with the observation that broader threshold distributions have larger homogenization volumes [15]. In our case, it is, however, likely that the crossover behavior

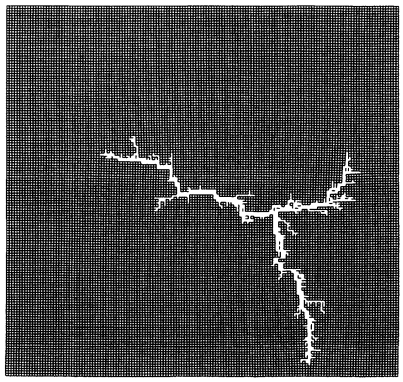

FIG. 3. Typical hydraulic crack for strong disorder, $r = -0.7$ and $\langle f_{coh} \rangle = 0.01$, on a lattice of size $L = 150$. The crack consists of 629 broken beams after 1500 time steps using a volume increment $\Delta V = 0.05$. The injection point is the center of the lattice. We have used periodic boundary conditions in vertical and horizontal directions.

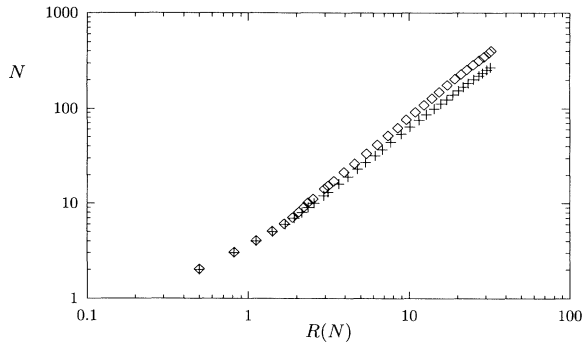

FIG. 4. Log-log plot of the number N of broken beams versus the radius of gyration $R(N)$ for two different distributions of breaking thresholds: ($\diamond$) $r = -0.7$, averages over 60 cracks, fractal dimension $d_f = 1.44 \pm 0.10$; (+) $r = -0.5$, averages over 53 cracks, fractal dimension $d_f = 1.39 \pm 0.10$. For all simulations we have used a mean cohesion value $\langle f_{coh} \rangle = 0.01$ and a linear lattice size $L = 150$.

is an effect of the finite size of the lattice. It has been argued [15,16] that for logarithmically diverging threshold distributions, i.e., for $r = -1$, a fracture process essentially reduces to a percolation problem. We note that this is not necessarily the case here because the breaking law employed is *asymmetric* with respect to tension and compression.

V. BURSTS AND TEMPORAL CORRELATIONS

Since the fractal nature is a fingerprint for infinite-range correlations in the crack geometry, one can also ask how the breaking events are correlated in *time*. To illustrate this question, we show in Fig. 5 the complete breaking sequence of the crack displayed in Fig. 3. We have plotted the number of beams broken between two consecutive time steps as a function of time. Most striking is the fact that the breaking process is very discontinuous in time. There are large time intervals in which no breaking occurs at all. During such time intervals of *quiescence* all beams on the crack surface are stressed below their cohesion thresholds and the acting pressure increases linearly in time. The second striking fact is that if a breaking event happens after a period of quiescence it usually triggers a sequence of consecutive breaking events (temporal clustering). We will call such sequences *bursts*. The bursts themselves are, as one can see in Fig. 5, unequally distributed in time. They occur relatively often for small times and become more rare later. However, while the bursts are narrow for early time steps they typically become broader with increasing time. The numbers of simultanously broken beams per time step also exhibit particularities. Let us call these numbers the *magnitudes* of the breaking events. Broad bursts typically consist of few events of high magnitude and much more of low magnitude. Figure 6 shows the magnifications of two bursts from Fig. 5. The ordinate gives the number of simultanously broken beams during a time step and the corresponding "released energies" as well. The definition of the released energies is given below in Sec. VI. We see that the peak energy releases do *not* temporarly coincide with the peak numbers of broken beams. In Fig.

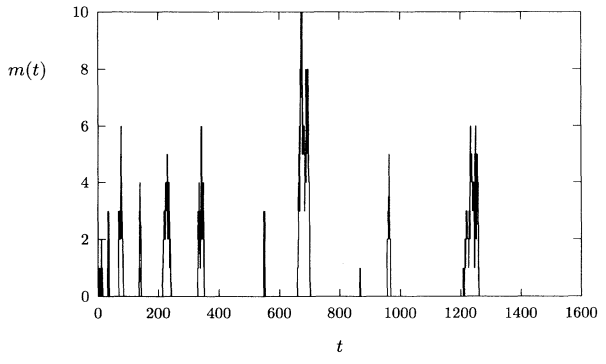

FIG. 5. Record of the breaking sequence in time corresponding to the crack displayed in Fig. 3. In this plot we have defined the magnitude $m(t)$ as the number of simultanously broken beams at a given unit time interval. The simulation stopped after 1500 time steps. Note the temporal clustering of breaking events and the large time intervals of quiescence.

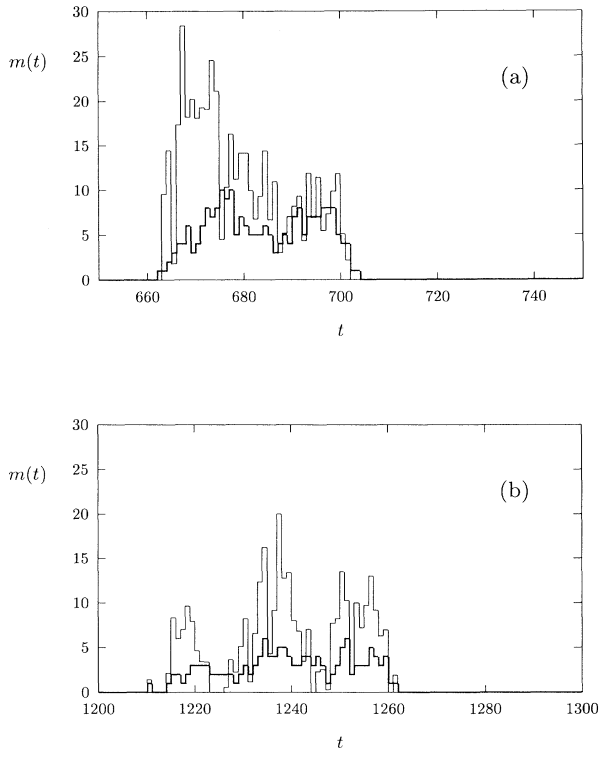

FIG. 6. Magnification of two bursts from Fig. 5, (a) at time $t \approx 650$ and (b) at time $t \approx 1210$. We have plotted the number $m(t)$ of simultanously broken beams (thick line) as well as the corresponding released energies δU (thin line) (compare Sec. VI for the definition of δU). The energies have been scaled by a constant factor.

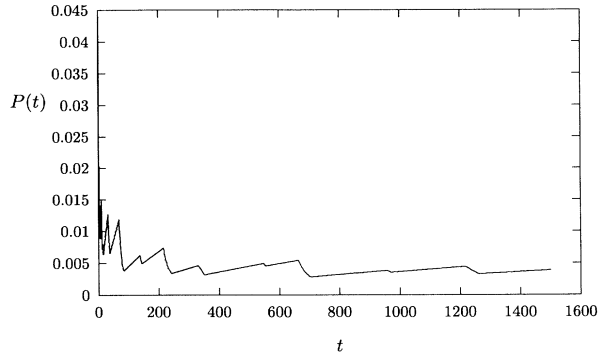

FIG. 7. Linear plot of the pressure P inside the crack versus time t. The pressure was obtained from the simulation corresponding to Fig. 5.

7 we show the time dependent pressure belonging to the breaking processes shown in Figs. 5 and 3, respectively.

The reader familar with magnitude records of earthquakes or of accoustic emission records from laboratory experiments will recognize some resemblance to our data.

In the following, we will investigate more closely the temporal clustering of breaking events. We have calculated the lifetime τ for each burst as the time that elapses between the first and the last breaking event of a burst. Figure 8 shows the (unnormalized) histogram of *burst lifetime* in a double logarithmic plot. Small bursts occur relatively often while larger bursts are less frequent. The statistics are made over 729 bursts from 60 samples for $r = -0.7$ and over 862 bursts from 53 crack simulations for $r = -0.5$. The largest detected burst has a lifetime of approximately $\tau = 140$. We note that for large lifetimes, $\tau \geq 30$, the statistic becomes unreliable because the occurrences, $n(\tau)$, become too small, $n(\tau) < 10$. This is also due to the fact that all simulations were stopped after $t_{max} = 1500$ time steps. In order to extract more information from the lifetime distribution, we consider in Fig. 9 the less noisy cumulative probability distribution $p(\tau)$ that a given burst has a lifetime shorter than or equal to τ. With an intermediate range we observe in Fig. 9 that the cummulative probability $p(\tau) = \sum_{i=1}^{\tau} n(i) / \sum_{i=1}^{t_{max}} n(i)$ seems to obey a power law $p(\tau) \propto \tau^{1-\eta}$ with $\eta = 0.54 \pm 0.15$. Hence, the lifetime distribution of bursts also follows a power law in this regime,

$$n(\tau) \propto \tau^{-\eta}. \tag{2}$$

It is remarkable that the two curves in Fig. 9 give nearly the same exponent η although the exponents r from their threshold distribution are different. This indicates that the underlaying generating mechanism for the temporal clustering of breaking events might be universal. In Fig. 9 one also sees strong deviations from the power law for small ($\tau < 4$) and for large ($\tau > 30$) bursts, particularly in the case of $r = -0.7$. The existence of an upper cutoff is plausible, because we stopped each crack growth after $t_{max} = 1500$ time steps. This artificially lowers the number of large bursts. The lower cutoff is quite common in cluster statistics, known as "corrections to scaling."

Next we consider the lifetime distribution $q(\tau)$ of *quiet intervals*. This distribution characterizes the arrangement of bursts on the natural time scale t and has attracted interest in seismology because of its possible role in predicting earthquakes [17]. It has been observed that if certain regions undergo high magnitude earthquakes they often show thereafter rather long periods of seismic quiescence (inactivity). We have investigated this statistic from our hydraulic fracturing calculations. In Fig. 10 we consider in a semilog plot the cumulative probability $Q(\tau)$ that two *consecutive* bursts are separated by a time interval of quiescence shorter than or equal to τ. More precisely, we define the width of the interval τ by the number of breaking free time steps between two consecutive bursts. For intermediate time scales the probability follows, as shown in Fig. 10, a logarithmic dependence, $Q(\tau) \propto \ln \tau$. Thus, the probability $q(\tau)$ of finding a quiet time interval of width τ between two adjacent bursts scales in this regime as

$$q(\tau) \propto \frac{1}{\tau}. \tag{3}$$

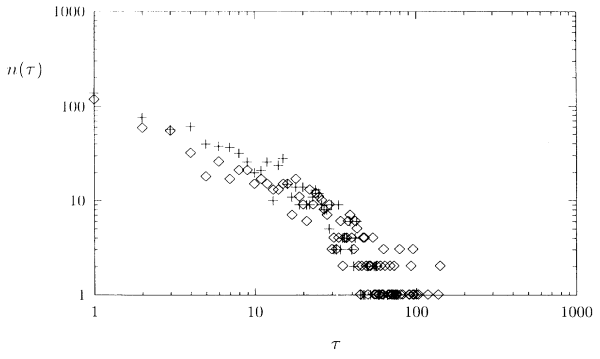

FIG. 8. Histogram for the burst lifetime τ in a double logarithmic representation. The occurrences $n(\tau)$ for bursts of size τ have been calculated for $r = -0.7$ ($\diamond$) and for $r = -0.5$ (+). The largest detected burst is of size $\tau = 140$. The simulations have been stopped after $t_{max} = 1500$ time steps.

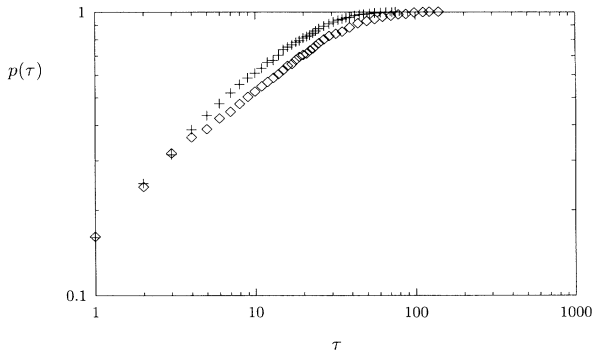

FIG. 9. Log-log plot of the cumulative probability distribution $p(\tau)$ that a burst selected at random is shorter τ. The distribution follows a power law, i.e., $p(\tau) \propto \tau^{1-\eta}$ with $\eta = 0.54 \pm 0.15$ for intermediate burst lifetimes. Symbols and parameters as in Fig. 8.

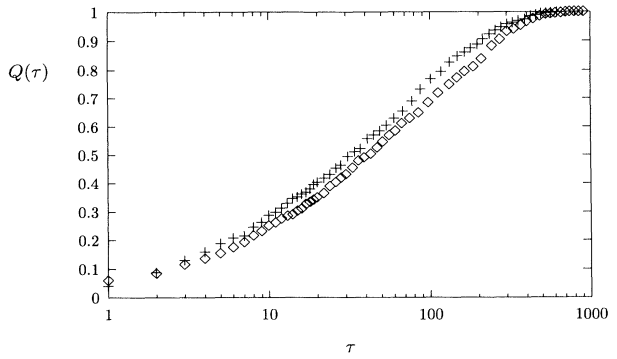

FIG. 10. Semi-log plot for the cumulative probability $Q(\tau)$ of finding between two adjacent bursts an emission (breaking) free time interval τ. Note the logarithmic dependence, $Q(\tau) \propto \ln \tau$, i.e., the probability $q(\tau)$ of finding a quiet interval of size τ scales as $q(\tau) = \partial_\tau Q \propto 1/\tau$. Symbols and parameters as in Fig. 8.

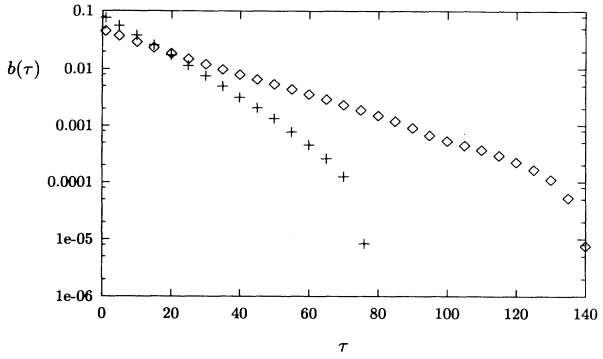

FIG. 11. Probability distribution $b(\tau)$ of finding two breaking events being τ time steps apart and *belonging to the same burst.* From the semilog plot one sees exponentially decreasing correlations, $b(\tau) \propto \exp(-a\tau)$. Symbols and parameters as in Fig. 8.

Interestingly, both distributions $n(\tau)$ and $q(\tau)$ scale for intermediate times as power laws, however, with different exponents.

So far we have considered the lifetime statistics of bursts and of quiet intervals. Valuable information about the temporal evolution of hydraulic cracks can be gained by considering the time correlations between the breaking events. *A priori* it is not obvious which of the breaking events are causally connected. In our model the elementary consecutive breaking events define the shortest accessible time scale. From acoustic emission experiments and seismic records, however, the existence of background noise is well established. Events are usually only considered if their magnitude exceeds the background noise by orders of magnitude [13,18]. The cutoff of the background noise leads to discrete magnitude-time sequences. This is similar in our model because the discrete nature of the beams establishes a lower cutoff for the possible size of an event. Experimentally, the variations in emission magnitudes are so strong and the line-widths are so small that one can consider acoustic emission "events" as δ peaks. We note that in experiments the significant breaking events are already temporal clusters (bursts). Hence, one can investigate the time correlations on the scale of a typical line width (burst lifetimes) or on a larger time scale. First we will investigate the case in which only correlations *within* the bursts are considered. We have calculated from all bursts the probability distribution $b(\tau)$ of time intervals $\tau = |t_i - t_j|$ between all possible pairs of breaking events belonging to the *same* burst. We show in Fig. 11 in a semilogarithmic plot the distribution of time intervals τ. One clearly sees an exponentially decreasing probability (two-point correlation) in time, $b(\tau) \propto \exp(-a\tau)$. In this plot one does not find any power-law behavior for small times, $\tau \leq 30$, as one might expect from the power-law scaling of burst lifetimes; see Eq. (2). In our case, this is due to the fact that the "large" bursts ($\tau > 30$), having unfavorable statistics, completely dominate the correlations also for small τ. This appears to be an additional complication resulting from the *very broad* lifetime distribution $n(\tau)$ of bursts, i.e., the small value of the exponent $\eta \approx 0.5$. We can, however, as discussed above, consider the correlations between all breaking events regardless of the bursts they belong to. This is conveniently done [10] by calculating the histogram of time intervals τ between *all possible pairs* of breaking events $\tau = |t_i - t_j|$ from a given time record. In Fig. 12 we show in a double logarithmic representation the normalized histogram of these time intervals. We find that the probability $g(\tau)$ of detecting two breaking events seperated by a time interval τ decreases on intermediate scales ($15 < \tau < 130$ for $r = -0.7$) as a power law,

$$g(\tau) \propto \tau^{-\kappa}, \quad \kappa = 0.94 \pm 0.20. \tag{4}$$

This corresponds to Omori's well known law of aftershocks which was first formulated in 1894 for earthquakes [19]. It says that the probability of an aftershock following a large earthquake decays as $1/\tau^\kappa$ in time with an exponent κ close to one. Omori's law has been verified

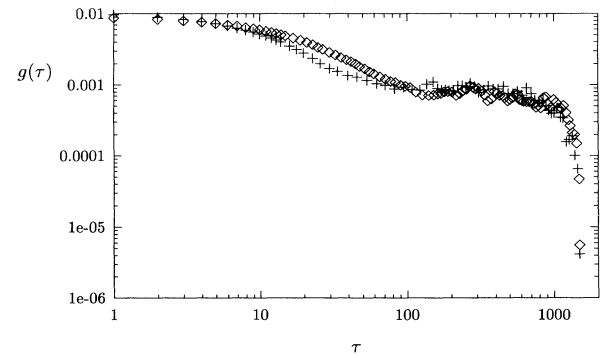

FIG. 12. Probability distribution $g(\tau)$ of finding two breaking events to be τ time steps apart. The distribution follows, for intermediate time scales, a power law (Omori's law) $g(\tau) \propto \tau^{-\kappa}$ with the value $\kappa = 0.94 \pm 0.20$. Symbols and parameters are the same as in Fig. 8.

from earthquake catalogs for aftershocks series ranging from a few hours to a couple of years after the main event. The empirical value of the exponent κ lies between 1.0 and 1.4 [10]. Although the appearance of earthquakes and aftershock series depends on quite different underlying constraints concerning the rheology and the crack opening mode than our two-dimensional model, we find a value for κ very close to the empirical one in three dimensions. Recently, it has been argued [18] that the value $\kappa = 1$ should hold quite generally for nonlinear fracture problems, such as earthquakes, independent of the spatial dimension [20]. Hence, one might expect the basic mechanism for burst sequences, or, respectively, aftershocks, to be *universal* due to *self-organization* of rupture. Physically one might argue that a main breaking event with high magnitude triggers smaller magnitude events which in turn create even smaller events *ad infinitum* if the cohesion properties are sufficient heterogeneous. However, in our case during a single burst the solid undergoes a quite complicated stress redistribution process until all microstructural elements (beams) are below their cohesion threshold. When the crack grows into new regions it may be stopped due to a region with particular high breaking thresholds. Then the burst terminates. As the crack becomes longer its critical opening volume necessary to overcome the thresholds increases even more because larger cracks can be opened more easily than small cracks. This explains why the intervals of quiescence become longer for larger cracks.

VI. RELEASED ENERGIES, ACOUSTIC EMISSION

So far we have considered the spatial and temporal correlations of breaking events during hydraulic fracturing. We have found qualitative and quantitative similarities to the seismic clustering of earthquakes and to acoustic emission laboratory experiments. However, we have so far not discussed the correlations of the magnitudes (intensities) of breaking events. For this the magnitude occurrence relationship is of central importance [21]. It has been found empirically that the cumulative occurrence $H(m)$ of earthquakes of magnitude larger than m follows the celebrated Gutenberg-Richter law, $H(m) \propto 10^{-bm}$ [22]. The b value found in the Gutenberg-Richter law is often close to one [10]. The magnitudes of seismic events are defined by the logarithmic wave amplitudes. The energy release δU is usually considered to be proportional to the squared amplitude of the earthquake. One typically obtains a cumulative occurrence-energy relation of the form $H(\delta U) \propto \delta U^{-0.6}$, expressing the presence of earthquakes on *all* energetical scales [11,21]. It has been shown recently [13] that acoustic emission in the ultrasonic frequency range due to microfracturing of synthetic plaster also exhibits a power law for the cumulative occurrences with an exponent close to the one found in the Gutenberg-Richter law. Similar finding from AE records have been published earlier for the microfracturing of rocks [23].

In the following, we will discuss some energetical aspects of our model. The thermodynamical description of crack spreading phenomena in heterogeneous environments becomes quite complicated and we will calculate the involved energies exclusively from the mechanical equilibrium conditions and *not* from thermodynamical considerations. In order to determine in our model the amount of energy released by a given breaking event one has to calculate the stored elastic energy $U(t)$ at each time step. This energy is, as already mentioned, determined prior to breaking from the sum over the energies of all nonbroken beams. We define the rate of change of elastic energy as $\delta U = -\partial U/\partial t = -(U(t+1) - U(t))$. If the rate δU is negative, then the lattice has increased its elastic energy. We have verified that the overwhelming majority of breaking events are detectable by the condition $\delta U > 0$. There are very few events that show a negative energy flux because the value of δU describes the sum of two effects. First, it describes the lowering of elastic energy due to a breaking event. Second, it describes the increase of elastic energy due to the added amount ΔV of fluid per time step. However, if the cracks and their corresponding opening volumes become large compared to ΔV, the fraction of nondetected events becomes very small. Experimentally the energy dissipation due to crack growth has at least two contributions. On one hand the creation of additional crack surface consumes energy. On the other hand elastic waves are emitted from the crack tip(s) (acoustic emission). Because we do not consider the full dynamic equations, it is *a priori* not clear which fraction of the dissipated energy to assign to the "acoustic emission." We propose that, as a first approximation, the AE energy per event is proportional to the rate of change of elastic energy δU of the system. We show in Fig. 13 in a semilog plot the cumulative occurrence $H(\delta U)$ of breaking events of energetical magnitude larger than δU. We find an exponential relationship,

$$H(\delta U) \propto \exp(-\beta \delta U). \tag{5}$$

The flat tail for large δU is due to low statistics. This result is at variance with what is expected from the Gutenberg-Richter law and AE measurements in laboratory experiments. A possible source of this discrepancy

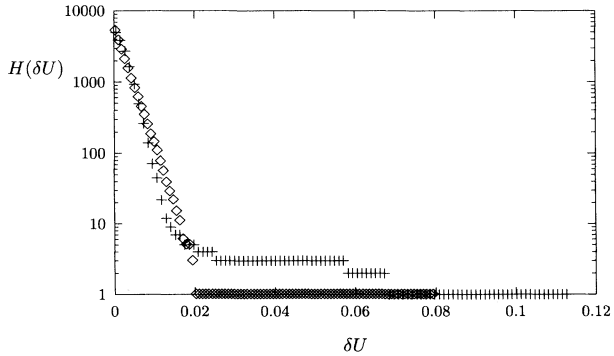

FIG. 13. Semilogarithmic plot for the cumulative occurrence $H(\delta U)$ that a given breaking event is of *energetical magnitude* larger than δU. We find for the cumulative occurrence an exponential decay $H(\delta U) \propto \exp(-\beta \delta U)$. Symbols and parameters as in Fig. 8.

could be our definition of the released energy: We proposed that the AE be proportional to the total energy relaxation. It could, however, be that the fraction of energy emitted acoustically is a more complicated function of the energy. Other sources of the deviations between our model and experiments could be the periodic boundary condition and the two dimensionality of the lattice used in our simulations.

VII. CONCLUSIONS

We have presented a lattice model for hydraulic fracture that takes into account the particular boundary conditions inside the hole and the quenched nature of the heterogeneities in the rock. We drive the process by increasing the crack volume linearly in time (constant flux). The pressure fluctuates erratically, similarly to what is measured at boreholes in the field. The crack shapes are fractal and the fractal dimension agrees well with measurements performed in Orlèans with Hele Shaw cells. The sequence of breaking events is organized in bursts that have a lifetime distribution and a distribution of quiescence times that are power laws. This indicates that self-organized criticality [24] takes place. Events inside a burst seem uncorrelated while long range correlations between bursts follow Omori's law for aftershocks. The distribution of released energies does not follow a power law within the numerical accuracy of our calculations, shedding doubts on the simple hypothesis that acoustic emission signals are simply proportional to the released potential energy.

This work is still rather preliminary if the full reality of hydraulic fracturing in oil or geothermal reservoirs is to be described. Real soils are three dimensional and the distribution of heterogeneities usually follows a Weibull distribution with a material dependent exponent. The pressure of the fluid in the crack is not constant but depends on the distance from the injection site and the geometry of the crack. The system is nearly infinite in size and the restrictions in the total volume of the system as imposed by the periodic boundary conditions are not realistic. Still many features have been found in this paper that agree with experimental measurements and we think that including more details into the model, which is rather straightforward, could help simulate hydraulic fracturing rather accurately in the future.

ACKNOWLEDGMENTS

One of us (F.T.) would like to thank E. C. Aifantis for useful discussions and would also like to gratefully acknowledge financial support from the Human Capital and Mobility program of the European Community under Grant No. ER-BCHBGCT 920041.

[1] H. Takahashi and H. Abé, in *Fracture Mechanics of Rock*, edited by B.K. Atkinson (Academic Press, London, 1987), p. 241.

[2] H. Van Damme, E. Alsac, and C. Laroe, C.R. Acad. Sci. Série II **309**, 11 (1989); H. Van Damme, in *The Fractal Approach to Heterogeneous Chemistry*, edited by D. Avnir (Wiley, New York, 1989) p. 199; E. Lemaire, P. Levitz, G. Daccord, and H. Van Damme, Phys. Rev. Lett. **67** 2009 (1991).

[3] E. Louis and F. Guinea, Europhys. Lett. **3**, 871 (1987); E. Louis, F. Guinea, and F. Flores, in *Fractals in Physics*, edited by L. Pietronero and E. Tossatti (Elsevier, Amsterdam, 1986); P. Meakin, G. Li, L.M. Sander, E. Louis, and F. Guinea, J. Phys. A **22**, 1393 (1989); E.L. Hinrichsen, A. Hansen, and S. Roux, Europhys. Lett. **8**, 747 (1988).

[4] H.J. Herrmann and J. Kertész, Physica A **178**, 227 (1991); H.J. Herrmann, in *Proceedings of the NATO workshop on Growth Patterns in Physical Sciences and Biology* edited by editors (Publisher, City, 1992).

[5] F. Tzschichholz, H.J. Herrmann, H.E. Roman, and M. Pfuff, Phys. Rev. B **49**, 7056 (1994).

[6] *Statistical Models for the Fracture of Disordered Media*, edited by H.J. Herrmann and S. Roux (North Holland, Amsterdam, 1990).

[7] M. Sahimi and J.D. Goddard, Phys. Rev. B **33**, 7848 (1986); F. Family, Y.C. Zhang, and T. Vicsek, J. Phys. A **19**, L733 (1986); B. Kahng, G.G. Batrouni, S. Redner, L. de Arcangelis, and H.J. Herrmann, Phys. Rev. B **37**, 7625 (1988); S. Roux, A. Hansen, H.J. Herrmann, and E. Guyon, J. Stat. Phys. **52**, 251 (1988); L. de Arcangelis, A. Hansen, H.J. Herrmann, and S. Roux, Phys. Rev. B **40**, 877 (1989); A. Hansen, S. Roux and H.J. Herrmann, J. Phys. (Paris) **50**, 733 (1989); H.J. Herrmann, A. Hansen, and S. Roux, Phys. Rev. B **39**, 637 (1989); L. de Arcangelis and H.J. Herrmann, Phys. Rev. B **39**, 2678 (1989); F. Tzschichholz, Phys. Rev. B **45**, 12 691 (1992); E. Schlangen and J.G.M. Van Mier, Mat. Struct. **25**, 534 (1992).

[8] G. G. Batrouni and A. Hansen, J. Stat. Phys. **52**, 747 (1988).

[9] From continuum mechanics one obtains the relation between the crack volume V, the acting pressure P, and the crack length $2R$, $V = \frac{2E}{\pi} PR^2$ in $d = 2$. On the other hand, Griffith's criterion for brittle fracture predicts a relation for the equilibrium pressure of the form $P_{crit} = \sqrt{\frac{2E\gamma_0}{\pi R}}$, where E and γ_0 denote the Young modulus and the specific surface energy, respectively. [See, for example, I. Sneddon and M. Lowengrub, *Crack Problems in the Classical Theory of Elasticity* (SIAM, Philadelphia, 1969)]. By eliminating the crack length from above relations one obtains the mentioned relation $P_{crit} \sim V^{-1/3}$ for an infinite system.

[10] See, for example, L. Knopoff in *Disorder and Fracture*, edited by J. Charmet *et al.* (Plenum Press, New York, 1990), pp. 279–87, and references therein.

[11] G. Korvin, in *Fractal Models in the Earth Sciences* (Elsevier, Amsterdam, 1992) pp. 156–67, and references therein; D.L. Turcotte, *Fractals and Chaos in Geology and Geophysics* (Cambridge University Press, Cambridge, 1992).

[12] I.G. Main, P.R. Sammonds, and P.G. Meredith, Geophys. J. Int. **115**, 367 (1993); C.G. Hatton, I.G. Main, and P.G.

Meredith, J. Struct. Geol. **15**, 1485 (1993).
[13] A. Petri, G. Paparo, A. Vespignani, A. Alippi, and M. Costantini (unpublished).
[14] H. Takahashi, H. Niitsuma, K. Tamakawa, H. Abé, R. Sato, and M. Suzuki (unpublished); J. N. Albright and C. F. Pearson, Soc. Petrol. Eng. J., **xx**, 523, (1982); H. Niitsuma, K. Nakatsuka, N. Chubachi, H. Yokoyama, and M. Takanohashi, Geothermics **14**, 525, (1985); H. Niitsuma, Int. J. Rock Mech. Min. Sci. Geomech. Abstr. **26**, 169, (1989).
[15] A. Hansen, in *Statistical Models for the Fracture of Disordered Media* (Ref. [6]), pp. 115–158.
[16] S. Roux, A. Hansen, H.J. Herrmann, and E. Guyon, J. Stat. Phys. **52**, 237, (1988).
[17] S.L. Pepke, J.M. Carlson, and B.E. Shaw, J. Geophys. Res. **99**, 6769 (1994).
[18] B.E. Shaw, Geophys. Res. Lett. **20**, 907 (1993).
[19] F. Omori, J. Coll. Sci. Imper. Univ. Tokyo **7**, 111, (1894).
[20] Although the independence of $\kappa = 1$ from the spatial dimension d has not been stated explicitly in Ref. [18] it follows from the fact that the given physical arguments do not depend on d.
[21] J. Lomnitz-Adler, J. Geophys. Res. **98**, 17 745 (1993).
[22] G. Gutenberg and C.F. Richter, Ann. Geophys. **9**, 1 (1956); C.F. Richter, *Elementary Seismology* (W.H. Freeman and Co., San Francisco, 1958).
[23] C.H. Scholz, Bull. Seismol. Soc. Am. **58**, 1117 (1968); C.J. Allègre, J.L. Le Mouel, and A. Provost, Nature **297**, 47 (1982); C.H. Scholz, Nature **338**, 459 (1989).
[24] P. Bak, C. Tang, and K. Wiesenfeld, Phys. Rev. Lett. **59**, 381 (1987).